

# PCCP

Accepted Manuscript



This is an *Accepted Manuscript*, which has been through the Royal Society of Chemistry peer review process and has been accepted for publication.

*Accepted Manuscripts* are published online shortly after acceptance, before technical editing, formatting and proof reading. Using this free service, authors can make their results available to the community, in citable form, before we publish the edited article. We will replace this *Accepted Manuscript* with the edited and formatted *Advance Article* as soon as it is available.

You can find more information about *Accepted Manuscripts* in the [Information for Authors](#).

Please note that technical editing may introduce minor changes to the text and/or graphics, which may alter content. The journal's standard [Terms & Conditions](#) and the [Ethical guidelines](#) still apply. In no event shall the Royal Society of Chemistry be held responsible for any errors or omissions in this *Accepted Manuscript* or any consequences arising from the use of any information it contains.



Journal Name

ARTICLE

## Thickness-dependent phase boundary in Sm-doped BiFeO<sub>3</sub> piezoelectric thin films on Pt/Ti/SiO<sub>2</sub>/Si substrates†

Wei Sun, Jing-Feng Li\*, Fangyuan Zhu, Qi Yu, Li-Qian Cheng and Zhen Zhou

Received 00th January 20xx,  
Accepted 00th January 20xx

DOI: 10.1039/x0xx00000x

www.rsc.org/

Sm-doped BiFeO<sub>3</sub> thin films were fabricated on platinized silicon substrates *via* the sol-gel method. Sm contents and thicknesses were varied in a wide range to investigate their effects on phase structure and piezoelectricity. X-ray diffraction and Raman spectroscopy experiments revealed a rhombohedral to orthorhombic phase transition and the co-existence of both phases in a certain compositional vicinity. It is found that the proportion of rhombohedral phase increased with film thickness at the compositions corresponding to the phase transition boundary, indicating the influence of film thickness on the phase structure. Phase transition phenomenon and film thickness effect on the boundary were also studied by piezoresponse force microscopy. Based on the structure analysis and piezoelectric characterization results, a phase diagram of thickness versus composition was proposed, in which morphotropic phase boundary located at 9% to 11% in thinner Sm-doped films and shifted towards Sm-rich side with increasing thickness.

### 1 Introduction

BiFeO<sub>3</sub> has been drawing prosperous attention as the only room-temperature multiferroic material discovered so far, which also manifests good photovoltaic and photocatalytic properties.<sup>1-5</sup> BiFeO<sub>3</sub> is reported to possess a high remnant polarization up to ~100 μC cm<sup>-2</sup>, so it is also expected to be one of the promising lead-free ferroelectric and piezoelectric materials with high Curie temperature ( $T_c \sim 830$  °C).<sup>1,2,6-8</sup> For piezoelectric materials, the morphotropic phase boundary (MPB) as firstly discovered in Pb(Zr,Ti)O<sub>3</sub> system is fundamentally important because of its existence resulting in a two-phase co-existing state for enhancing piezoelectricity.<sup>9,10</sup> Additionally, compositions at MPB where two different phase structures are both thermodynamically stable and more flexible polarization orientations are brought in for the co-existence of the mixed phases.

Recent studies have been devoted to the rhombohedral-orthorhombic (*R-O*) phase transition, which is induced by the rare-earth element substitution at A-site of BiFeO<sub>3</sub>. The smaller radius of rare-earth elements than that of Bi were thought to be the origin of the phase transition.<sup>11-15</sup> For the Sm-substituted BiFeO<sub>3</sub>, Takeuchi *et al.* reported that the MPB position is located at 14% Sm where *R3c*, a PbZrO<sub>3</sub>-like phase and *Pnma* coexist, and the phenomenon of antiferroelectric property was ascribed to the PbZrO<sub>3</sub>-like anti-polar phase. These works were mainly based on thin films grown on SrTiO<sub>3</sub> by pulse laser deposition (PLD) method.<sup>15-18</sup> Most recently,

similar phase transition was also discovered in sol-gel-processed Sm-doped BiFeO<sub>3</sub> thin films on conventional Pt/Ti/SiO<sub>2</sub>/Si wafers, which has been widely used in microelectronic devices nowadays.<sup>19</sup> However, the compositional location of MPB in the sol-gel-processed thin films grown on Pt/Ti/SiO<sub>2</sub>/Si is not consistent with the reported SrTiO<sub>3</sub> substrate ones by PLD method. Obviously, it indicates the complexity of phase structures in Sm-doped BiFeO<sub>3</sub> thin films. Actually, the previous studies showed that the phase structures of Pb(Zr,Ti)O<sub>3</sub>-based piezoelectric thin films might differentiate from that in bulk materials even for the same composition and hence the shifting of phase boundary could occur in the films due to the substrate's clamping effect.<sup>20,21</sup> Furthermore, it has been reported that a rhombohedral-tetragonal MPB can be created by strain engineering in epitaxially grown BiFeO<sub>3</sub> thin films on single crystal substrates.<sup>3,22-25</sup> Generally, the clamping effect in non-epitaxial thin films on silicon wafers should be weaker as compared with epitaxial ones, but it is also quite significant to the identical phase transition within certain range of compositions in the doped BiFeO<sub>3</sub> thin films.

In this work, we prepared a series of Sm-doped BiFeO<sub>3</sub> thin films of a wide Sm content range from 9% to 15% with various thicknesses on platinized silicon substrates *via* a sol-gel method. *R-O* phase transition was found with increasing Sm contents but the phase boundaries were thickness-dependent. Piezoelectric test was performed and demonstrated the MPB behaviours. A thickness-composition phase diagram was proposed based on the experiments and a thermal contraction model was illustrated to explain the thickness dependent phase boundary.

### 2 Experimental

#### Synthesis

State Key Laboratory of New Ceramics and Fine Processing, School of Materials Science and Engineering, Tsinghua University, 100084 Beijing, P. R. China. E-mail: jingfeng@mail.tsinghua.edu.cn

† Electronic Supplementary Information (ESI) available: Fig. S1-S4. See DOI: 10.1039/x0xx00000x

Bismuth nitrate [Bi(NO<sub>3</sub>)<sub>3</sub>·5H<sub>2</sub>O] (99.99%), samarium nitrate [Sm(NO<sub>3</sub>)<sub>3</sub>·6H<sub>2</sub>O] (99.9%) and iron nitrate [Fe(NO<sub>3</sub>)<sub>3</sub>·9H<sub>2</sub>O] (99.99%) were used as the starting materials and dissolved into 2-methoxyethanol and citric acid (99.995%) was then added as the chelating agent. The mixed solution was stirred for 4 h at room temperature and then aged for 72 h. The solutions corresponding to 9-15% Sm-doped BiFeO<sub>3</sub> were prepared in this way and 7% bismuth was added in each solution to compensate for the loss during the heat treatment. The solutions were deposited onto Pt/Ti/SiO<sub>2</sub>/Si substrates by spin coating and then dried at 100 °C, pyrolyzed at 380 °C and annealed at 550 °C in an ambient atmosphere. After going through the deposition-pyrolysis-annealing process, one layer of Sm-doped BiFeO<sub>3</sub> was deposited onto the substrate with a thickness of ~60 nm according to scanning electron microscopy (SEM) observation. For each composition, this process was repeated for one to seven times to prepare the samples with multiple thicknesses. The sample with *x* mole percent Sm and *y* nm thickness was represented as BS*x*F-*y*nm for abbreviation in the following sections.

### Characterization

The crystallographic structure of thin films was characterized by X-ray diffraction (XRD, D/max-RB, Rigaku) using Cu-K<sub>α</sub> radiation (λ=1.5406Å). Step scanning of {200}<sub>pc</sub> peaks was performed at the BL14B1 Beamline of Shanghai Synchrotron Radiation Facility (SSRF) with λ=1.2398Å. Raman spectrum was performed on a Raman spectrometer (LabRAM HR Evolution, HIROBA) at the wavelength of 532 nm. The cross-section morphology was observed *via* a field-emission scanning electron microscope (FE-SEM, LEO1530). Rutherford backscattering spectrometry (RBS) measurement was performed with 2022 keV He<sup>+</sup> beam provided by the 5SDH-2 Tandem accelerator made by NEC at Peking University. The surface morphology and piezoelectric property were detected by using an atomic force microscope (AFM, MFP-3D, Asylum Research) with a functionality of piezoresponse force microscopy (PFM). A Pt-coated cantilever (Olympus AC240, nominal spring constant 2 N m<sup>-1</sup>, resonant frequency 70 kHz) was used with platinumized silicon substrates acting as the counter electrodes.

## 3 Results and Discussion

### Microstructure and morphology

According to XRD patterns, all the samples demonstrate only BiFeO<sub>3</sub> perovskite phases without impurities. Fig. 1(a)-(c) display the step scanning patterns of {200}<sub>pc</sub> peaks of BS10F, BS11F and BS12F samples with different thicknesses. Three space groups, *R3c*, *Pbam* and *Pnma*, have been reported in Sm-doped BiFeO<sub>3</sub> system.<sup>16,26</sup> The bars at the bottom indicate the ideal peak positions and intensities of {200}<sub>pc</sub> of different space groups.<sup>19</sup> Both rhombohedral (*R*) and orthorhombic (*O*) phases border each other at 36.8°. Due to weak intensity and peak broadening resulted from small grain size, it is difficult to distinguish *Pbam* from *Pnma*.

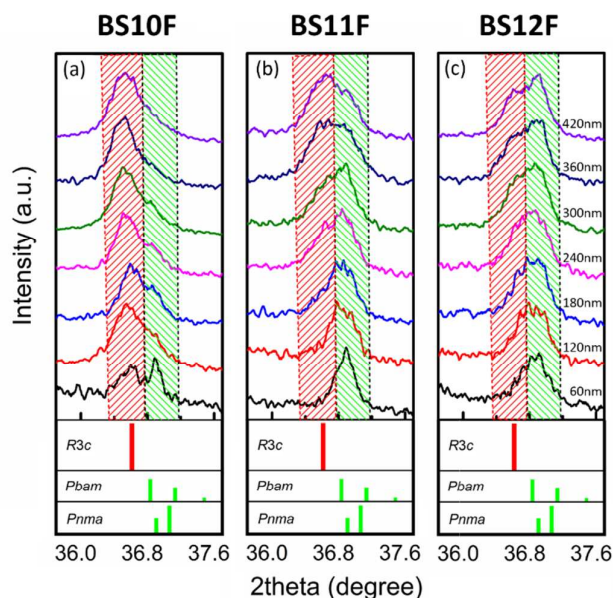
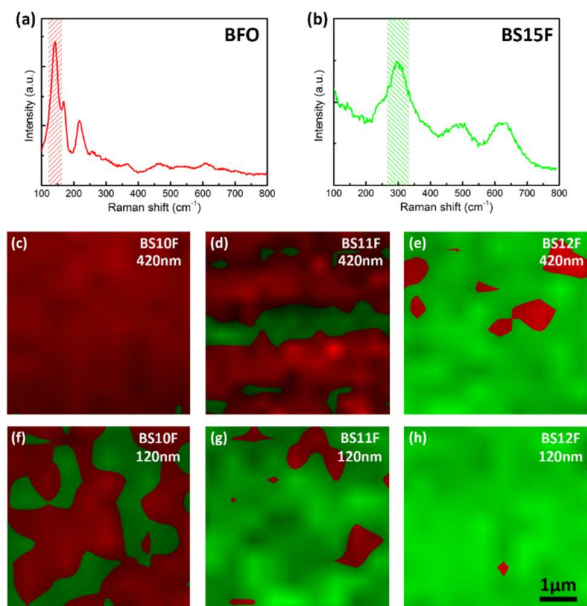


Fig. 1. XRD profiles of step scanning of {200}<sub>pc</sub> peaks from (a) BS10F, (b) BS11F and (c) BS12F with various thicknesses. Histograms in the bottom indicates the ideal peak positions of {200}<sub>pc</sub> in *R3c*, *Pbam* and *Pnma*. Contributions from *R* and *O* phase are indicated by red and green diagonal lines respectively.

For the BS10F composition, the peaks from both phases were detected at the film thickness of 60 nm. As thickness increases, the left peak becomes stronger while the right peak becomes weaker. For the thickness larger than 120 nm, the intensity of left peak is always stronger than the right peak; the *O* phase almost disappears for the films over 300 nm. For the BS11F samples with 11% Sm, only *O* phase exists in 60-nm-thick film. *R* phase emerges in the films thicker than 180 nm. It can be regarded as that both *R* and *O* phases exist in these samples, whereas the proportion of *R* phase is higher than that of *O* phase in 360-nm-thick and 420-nm-thick films since the left peak is more intensive than right one. However, for the BS12F samples, *R* phase existed only when the film thickness exceeds 300 nm with *O* phase being dominating in all the samples. It is worthwhile noting that similar XRD peaks could be found among all three compositions by only changing the film thickness. For example, the peak shape of BS11F-420nm is very similar to the case of BS10F-180nm, and the peak shape of BS12F-420nm is the same with BS11F-240nm. Therefore, it is clearly indicated that the phase structures are fundamentally affected by the film thickness in the Sm-doped BiFeO<sub>3</sub> films. For the films with lower Sm content like BS9F samples, the XRD patterns revealed that *R* phase is the majority, being similar to that of BS10F-420nm shown in Fig. 1. On the other hand, when Sm contents are over 13%, only *O* phase was observed, whose XRD patterns are similar to BS12F-60nm sample shown in Fig. 1. The XRD results revealed that the phase transition from *R* to *O* occurs at 10% to 12% Sm doping contents. Both phases can be found in the same sample, which suggests an MPB region.



**Fig. 2.** Raman spectrum of (a) BFO and (b) BS15F thin films; (c)-(h) Raman maps collected from (c) BS10F-420nm, (d) BS11F-420nm, (e) BS12F-420nm, (f) BS10F-120nm, (g) BS11F-120nm and (h) BS12F-120nm. Limits were set in the Raman shift between approximately 120 to 160  $\text{cm}^{-1}$  and 260 to 320  $\text{cm}^{-1}$  to define contributions from the *R* and *O* phases respectively.

Raman spectroscopy is effective in distinguishing tiny differences in phase structure. To assure the MPB position, Raman spectroscopy mapping was done on six film samples with three compositions (BS10F, BS11F and BS12F) and two thicknesses (120 nm and 420 nm). For reference, Fig. 2(a) and 2(b) show the Raman spectra of BiFeO<sub>3</sub> (BFO) which possesses a *R3c* distorted perovskite structure and BS15F which has an orthorhombic distorted perovskite structure, respectively.<sup>27,28</sup> The strongest peaks correspond to *A<sub>g</sub>-1* and *A<sub>g</sub>-4* vibration modes in *R* and *O* phases, respectively, which were used as an indicator for each phase. During the Raman mapping, limits were set in the Raman shift from approximately 120 to 160  $\text{cm}^{-1}$  and 260 to 320  $\text{cm}^{-1}$  to define contributions from *R* and *O* phase respectively, as were hatched in Fig. 2(a) and 2(b).<sup>13</sup> Then Raman spectra were collected in 5  $\mu\text{m} \times 5 \mu\text{m}$  area from 100 points for selected samples and the results are shown in Fig. 2(c)-(h). The area with more *R* phase contributions is marked as red while that with more *O* phase is marked as green. It should be emphasized that the colour separation does not mean phase segregation. Raman mapping results in a phase-mixed appearance are shown in Fig. S1.

Fig. 2(c) and 2(h) are Raman mapping results of BS10F-420nm and BS10F-120nm, respectively. It should be noted that colours in the figures just represent the phase whose intensity is higher at certain point than the other phase. The thicker film is of *R* phase across the entire scanned region, while in the thinner film the two phases have almost equal share. For BS11F, both phases can be found in 420 nm and 120 nm films.

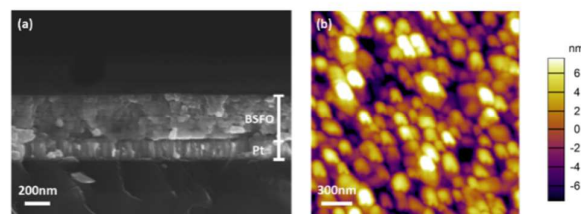


**Fig. 3.** (a) Cross-sectional SEM image and (b) surface morphology image of BS10F-420nm thin film.

Nevertheless, *R* phase is dominative in the thicker films but *O* phase is in the majority in the thinner films. For the composition of BS12F, almost a single *O* phase was found in the thinner film of 120 nm, but in the thicker film of 420 nm, *R* phase surpasses the *O* phase in some areas. From the Raman mapping results that both *R* and *O* phases were found in 10% to 12% Sm doping samples, the MPB position was again confirmed. It can be concluded that with increasing Sm content, the thin films tends to be *O* phase. For a fixed composition at MPB, the thicker the film is, the more *R* phase components there are.

The cross-sectional SEM image of BS10F-420nm sample is displayed in Fig. 3(a). The Sm-doped BiFeO<sub>3</sub> thin film is flat on surface and dense, and the polycrystalline structure on columnar platinum electrode can be seen clearly. Some regions showing layered structures might be related with the layer-by-layer coating process. Fig. 3(b) shows the surface topographic image of the same sample whose roughness is 4.2 nm. AFM images of BS10F samples with other thicknesses are displayed in Fig. S2, which again confirms the polycrystalline behaviour and the grain sizes are ~80 nm to 100 nm regardless of thickness. AFM images of other compositions also revealed the polycrystalline feature. The small differences on roughness and grain size among all the samples should have little influence on crystal structure and electric property.

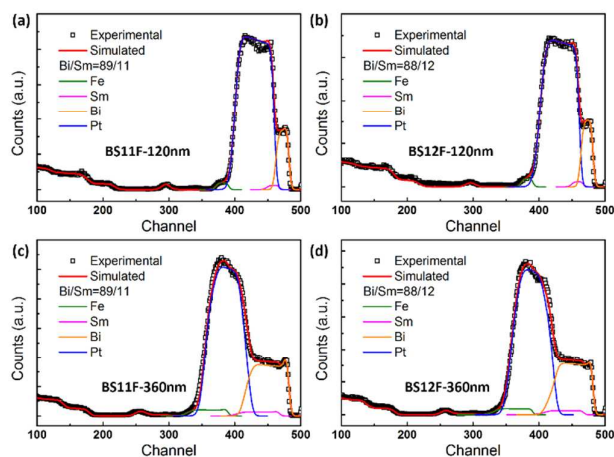


**Fig. 4.** RBS spectra of (a) BS11F-120nm, (b) BS12F-120nm, (c) BS11F-360nm and (d) BS12F-360nm thin films

RBS can provide quantitative results of elemental compositions and depth profiling of heavy elements without reference sample, besides, the measurement is non-destructive. We performed RBS on four samples: BS11F-120nm, BS12F-120nm, BS11F-360nm and BS12F-360nm, whose spectra together with computational simulations using the SIMNRA code are displayed in Fig. 4(a)-(d), respectively. The peaks at high energies (channel number) correspond to scatterings from the heavy elements, while the step at lower energy corresponds to scatterings from Si and O. According to simulation, signals contributed from Bi, Sm, Fe together with Pt electrode are depicted in the figures. The widths of the peaks are directly proportional to the thickness of the thin films. Experimental data are almost completely consistent with the simulation using nominal composition as shown in the figures, implying that the accurate constituents in these four samples agree well with raw materials. In addition, by comparing samples with the same composition and different thicknesses, it can be concluded that thickness had little influence on the elemental distribution of thin films.

### Piezoelectric response

PFM was used to attain direct evidence of piezoelectric response to assure the MPB position. The piezoelectric properties of Sm-doped BiFeO<sub>3</sub> thin films were characterized by using the local switching spectroscopy piezoresponse force microscopy (SS-PFM) technique. In this mode, a step-varying DC voltage ranging from -30 V to 30 V was applied to the sample to pole the ferroelectric films. During the PFM testing, a modulated AC voltage of 3 V was applied on the DC signal so that the resonant piezoelectric response was acquired.<sup>29-31</sup> The acquired signal includes two parts: amplitude and phase, which manifest butterfly loop and hysteresis loop as indicators of displacement and domain switching, respectively. The amplitude at  $\pm 30$  V represents the displacement of a sample when all the domains are switched, corresponding to the magnitude of reverse piezoelectric coefficient. The average value of this maximum displacement was calculated to denote the piezoelectric response of each sample. The piezoresponse test was performed within a  $2 \mu\text{m} \times 2 \mu\text{m}$  sized mesh of 144

points for all the samples to ensure the reliability of our comparison.

Four samples, BS9F-180nm, BS11F-420nm, BS13F-360nm and BS15F-120nm, were chosen for comparison with their amplitude and phase loops plotted in Fig. 5(a) and 5(b). XRD and Raman profiles of these four samples are presented in Fig. S4. For BS9F-180nm and BS11F-420nm, the amplitudes are much stronger than that of BS13F-360nm. Phase image reveals 180° contrast indicating complete polarization switching in these three samples. However, for BS15F-120nm sample, the phase signal shows no hysteresis loop and the amplitude signal is chaos implying no piezoelectric response in it. Asymmetric butterfly shape was found during the tests, particularly obvious in the BS13F-360nm sample. This may be due to the static electricity and imprint electric field originated from space charge accumulation.<sup>32</sup>

According to the relative intensity, the piezoelectric responses of the samples were drawn in a two-dimension colour filled graph as shown in Fig. 5(c). The four selected samples were denoted in the figure with the corresponding graphical symbols. It can be concluded that piezoelectric performances show good accordance with structure analysis that MPB gives rise to the piezoelectricity as denoted by light yellow band. Among samples of MPB region, the highest piezoelectric response was achieved at BS11F-420nm. This can be ascribed to the large thickness of this sample in which more effective volume deformed under electric field. Generally, a thicker film always reveals stronger piezoelectric response.<sup>33</sup> The very thin films with compositions of BS14F and BS15F display no piezoresponse. It can be reasonably estimated that these samples are entirely made up of *Pnma* phase, a centrosymmetric space group which demonstrates no ferroelectric and piezoelectric properties. For the samples belonging to *O* phase but manifesting piezoelectricity, such as BS13F, BS14F-360nm and BS14F-420nm, the phase structure may be *Pbam* or the combination of *Pbam* and *Pnma* or a more complex structure as will be discussed later.<sup>34,35</sup> It is worth noting that the phase boundary of *Pnma* region, where no piezoresponse was obtained, also leans towards right side, implying that the thickness effect plays an important role not only in MPB region, but in all the films.

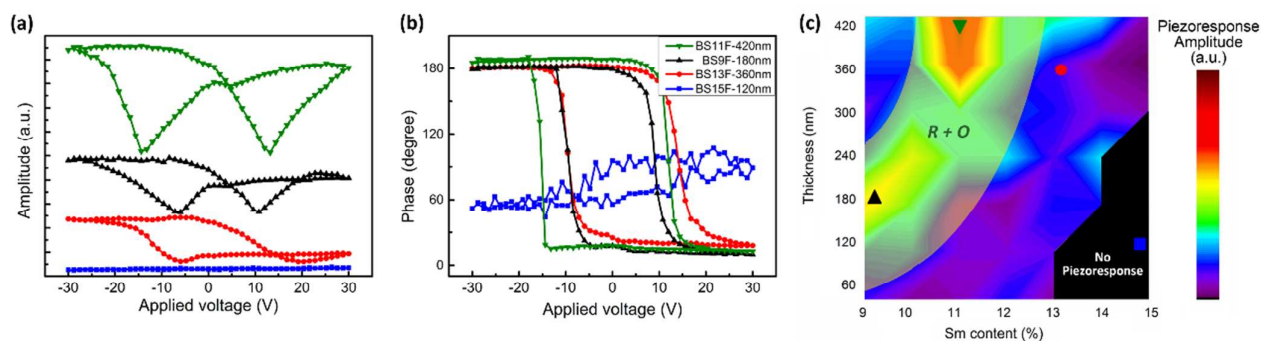


Fig. 5. (a) Amplitude and (b) phase loops of BS11F-420nm, BS9F-180nm, BS13F-360nm and BS15F-120nm. (c) Two-dimension colour filled graph of relative piezoelectric performance as functions of thickness and Sm contents. The yellow band indicates the MPB position and the four selected samples in (a) and (b) are also depicted with corresponding symbols.

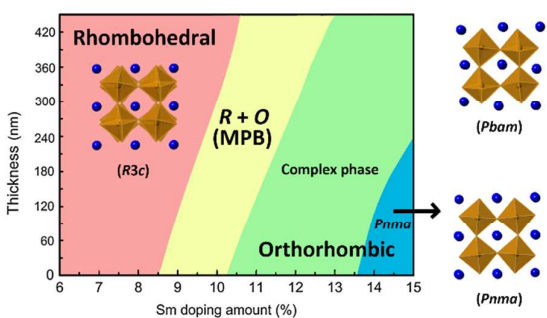


Fig. 6. Proposed schematic thickness-composition phase diagram for Sm-doped BiFeO<sub>3</sub> thin films with vertical viewings of R3c, Pbam and Pnma atomic structures embedded.

### Discussion of phase transition

Based on XRD, Raman and PFM results, here a schematic thickness-composition phase diagram is proposed and displayed in Fig. 6. The three kinds of crystal structures viewed along the pseudo-cubic [001] direction are also shown in the figure. Eight oxygen octahedrons are retained to clearly reveal the phase transition though they are not the complete unit cell.<sup>36</sup> The pink region at left side represents the rhombohedral phase and the space group is R3c. The yellow region in the centre corresponds to the MPB region in which both R and O phases coexist and the phase boundary leans toward right side. MPB locates at 9 to 11% in thinner films and shifts towards right side with increasing thickness and finally locates at 10% to 12% Sm doping contents at 420 nm. Deduced from piezoelectric properties, the blue region ranging from 14% to 15% in thinner films manifests paraelectric property and corresponds to the centrosymmetric phase Pnma, as can be seen from atomic structure in which the Bi atoms located in the centre of FeO<sub>6</sub> octahedrons. The phase boundary of Pnma is also a slanting one, indicating that the thickness effect prevails in all the compositions.

The green region is denoted as “complex phase” since we cannot determine the accurate structure based on existing experimental results. The XRD patterns suggest an orthorhombic phase and complete polarization switching indicates a non-centrosymmetric structure in this region. This complex phase was also discussed in other rare-earth-doped BiFeO<sub>3</sub> systems including Sm-doped BiFeO<sub>3</sub>.<sup>13,26,35,36</sup> A PbZrO<sub>3</sub>-like anti-polar phase has been proposed in rare-earth doped BiFeO<sub>3</sub> system, or sometimes denoted as Pbam space group whose vertical view is also drawn in Fig. 6.<sup>16-18</sup> However, we found no direct evidence, for example, the double hysteresis loop during PFM test to confirm the existence of antiferroelectricity.<sup>37</sup> Besides, the PbZrO<sub>3</sub>-like phase is unstable and tends to transform from R3c to Pbam or vice versa under different strain states.<sup>38</sup> Even if the complex phase was Pbam, there might be a region located beside the Pnma region in which Pbam and Pnma phases coexisted, but we could not figure it out yet. Further study is needed to determine the structure of this complex phase, yet

polycrystalline behaviour and phase segregation increase the difficulty.<sup>19,39</sup>

For the slanting phase boundaries of MPB and Pnma, compositional analysis by RBS has ruled out the possibility of compositional change for thin films with different thicknesses. Here we propose a phenomenological model concerning about thermal expansion coefficient to explain the thickness effect. The slanting phase boundary should be related with residual stress in the films. Since there is a big difference between the thermal expansion coefficient of Si ( $2.6 \times 10^{-6} \text{ K}^{-1}$ – $4.0 \times 10^{-6} \text{ K}^{-1}$ ) and BiFeO<sub>3</sub> ( $6.5 \times 10^{-6} \text{ K}^{-1}$ – $13 \times 10^{-6} \text{ K}^{-1}$ ),<sup>2</sup> resulting in an in-plane tensile thermal stress when the sample was cooled to room temperature after annealing for crystallization.<sup>20</sup> Besides, the in-plane tensile stress is equivalent to the out-of-plane compressive stress. This stress reserved in the films would be released gradually with increasing thickness. According to first-principles calculation, the in-plane tensile stress is in favour of O phase.<sup>40</sup> So compared with the reported 14% MPB position,<sup>15,18</sup> less Sm is needed to induce the phase transition in the present films. As thickness increases, the out-of-plane compressive stress and the in-plane tensile stress are released so that more Sm is needed to induce the R-O phase transition. It can be concluded that the MPB position is sensitive to the strain state of thin films. The constraint effect also works in the same way to shift Pnma phase boundary.

Fig. 7 shows the peak position of A<sub>g</sub>-4 mode of O phase (the peak overlapped by green stripes in Fig. 2(b)) in samples with different compositions and thicknesses. For BS9F samples of 300 nm and thicker, they demonstrate completely R phase and the A<sub>g</sub>-4 peak at 300 cm<sup>-1</sup> can hardly be seen so there are only 4 points for this composition. With increasing Sm contents, the A<sub>g</sub>-4 peak shifts towards higher wavenumber, corresponding to the stronger Sm-O bonding than Bi-O. The peak position of A<sub>g</sub>-4 shows an overall trend of shifting towards lower wavenumber with increasing thickness, corresponding to a decreasing out-of-plane compressive stress,<sup>41,42</sup> hence the model of stress relaxation was affirmed. Besides, as thickness increases, the XRD peaks of {200}<sub>pc</sub> also show a tendency of left shifting, indicating that the lattice constant increases along out-of-plane direction.

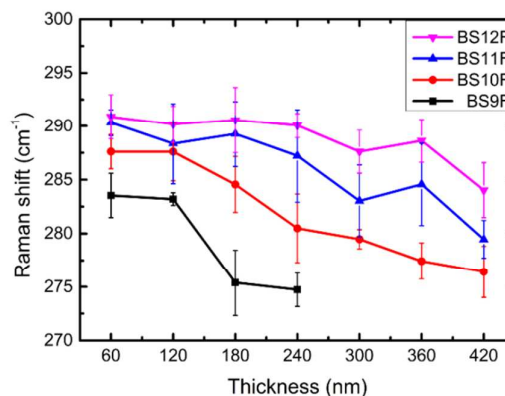


Fig. 7. Peak position of A<sub>g</sub>-4 mode of O phase in BS9F, BS10F, BS11F and BS12F samples.

Another possible explanation to the thickness effect is flexoelectricity since a strain gradient generates when stress is relaxed with thickness. Flexoelectric field will give rise to self-polarization and make contributions to the piezoelectric response. In thicker films, the contribution from flexoelectricity to the polarization is much greater than the clamping effect which plays a major role in thinner films.<sup>43</sup> What is more, the flexoelectricity can be applied to explain the imprinting field emerged during PFM tests.<sup>43</sup> Nevertheless, there is a lack of effective method to measure the flexoelectricity precisely by far.

## 4 Conclusion

In summary, 9% to 15% Sm doped BiFeO<sub>3</sub> thin films with various thicknesses ranging from 120 nm to 420 nm were fabricated via a sol-gel method. MPB was found at 9% to 12% Sm and the phase boundary is thickness-dependent. For thicker films, more Sm is needed to induce the phase transition. At MPB region, significantly enhanced piezoelectric performance was achieved. A thickness-composition phase diagram is presented based on XRD, Raman and PFM results. The slanting phase boundary can be related with the in-plane tensile thermal stress induced by the difference between thermal expansion coefficient of BiFeO<sub>3</sub> and substrates. Peak shifting of Raman vibration mode illustrated stress relaxation with thickness.

## Acknowledgements

This work was supported by National Nature Science Foundation of China (Grants no. 51332002, 51221291) the Ministry of Science and Technology of China under the Grant 2015CB654605. The authors would like to thank the Shanghai Synchrotron Radiation Facility for access to BL14B1 beamline under project nos. 13SRBL14B16671.

## Notes and references

- 1 J. Wang, J. B. Neaton, H. Zheng, V. Nagarajan, S. B. Ogale, B. Liu, D. Viehland, V. Vaithyanathan, D. G. Schlom, U. V. Waghmare, N. A. Spaldin, K. M. Rabe, M. Wuttig and R. Ramesh, *Science*, 2003, **299**, 1719.
- 2 G. Catalan and J. F. Scott, *Adv. Mater.*, 2009, **21**, 2463.
- 3 R. J. Zeches, M. D. Rossell, J. X. Zhang, A. J. Hatt, Q. He, C. H. Yang, A. Kumar, C. H. Wang, A. Melville, C. Adamo, G. Sheng, Y. H. Chu, J. F. Ihlefeld, R. Erni, C. Ederer, V. Gopalan, L. Q. Chen, D. G. Schlom, N. A. Spaldin, L. W. Martin and R. Ramesh, *Science*, 2009, **326**, 977.
- 4 J. T. Heron, J. L. Bosse, Q. He, Y. Gao, M. Trassin, L. Ye, J. D. Clarkson, C. Wang, J. Liu, S. Salahuddin, D. C. Ralph, D. G. Schlom, J. Iniguez, B. D. Huey and R. Ramesh, *Nature*, 2014, **516**, 370-373.
- 5 D. Sando, A. Barthelemy and M. Bibes, *J. Phys.: Condens. Matter.*, 2014, **26**, 473201.
- 6 J.-H. Lee, M.-A. Oak, H. J. Choi, J. Y. Son and H. M. Jang, *J. Mater. Chem.*, 2012, **22**, 1667.
- 7 A. Mukherjee, S. Basu, P. K. Manna, S. M. Yusuf and M. Pal, *J. Mater. Chem. C*, 2014, **2**, 5885.
- 8 N. Maso, H. Beltran, M. Prades, E. Cordocillo and A. R. West, *Phys. Chem. Chem. Phys.*, 2014, **16**, 19408.
- 9 G. H. Haertling, *J. Am. Ceram. Soc.*, 1999, **82**, 797.
- 10 N. Setter, D. Damjanovic, L. Eng, G. Fox, S. Gevorgian, S. Hong, A. Kingon, H. Kohlstedt, N. Y. Park, G. B. Stephenson, I. Stolitchnov, A. K. Tagansteve, D. V. Taylor, T. Yamada and S. Streiffner, *J. Appl. Phys.*, 2006, **100**, 051606.
- 11 J. Walker, B. Budic, P. Bryant, V. Kurusingal, C. Sorrell, A. Bencan, T. Rojac and N. Valanoor, *IEEE T. Ultrason. Ferr.*, 2015, **62**, 83.
- 12 S. Karimi, I. M. Reaney, Y. Han, J. Pokorny and I. Sterianou, *J. Mater. Sci.*, 2009, **44**, 5102.
- 13 R. C. Lennox, M. C. Price, W. Jamieson, M. Jura, A. Daoud-Aladine, C. A. Murray, C. Tang and D. C. Arnold, *J. Mater. Chem. C*, 2014, **2**, 3345.
- 14 M. Muneeswaran and N. V. Giridharan, *J. Appl. Phys.*, 2014, **115**, 214109.
- 15 C. H. Yang, D. Kan, I. Takeuchi, V. Nagarajan and J. Seidel, *Phys. Chem. Chem. Phys.*, 2012, **14**, 15953.
- 16 S. B. Emery, C. J. Cheng, D. Kan, F. J. Rueckert, S. P. Alpay, V. Nagarajan, I. Takeuchi and B. O. Wells, *Appl. Phys. Lett.*, 2010, **97**, 152902.
- 17 D. Kan, V. Anbusathaiah and I. Takeuchi, *Adv. Mater.*, 2011, **23**, 1765.
- 18 D. Kan, C. J. Long, C. Steinmetz, S. E. Lofland and I. Takeuchi, *J. Mater. Res.*, 2012, **27**, 2691.
- 19 W. Sun, J.-F. Li, Q. Yu and L.-Q. Cheng, *J. Mater. Chem. C*, 2015, **3**, 2115.
- 20 Z.-X. Zhu, C. Ruangchalermwong and J.-F. Li, *J. Appl. Phys.*, 2008, **104**, 054107.
- 21 J.-F. Li, Z.-X. Zhu and F.-P. Lai, *J. Phys. Chem. C*, 2010, **114**, 17796.
- 22 C. Beekman, W. Siemons, T. Z. Ward, M. Chi, J. Howe, M. D. Biegalski, N. Balke, P. Maksymovych, A. K. Farrar, J. B. Romero, P. Gao, X. Q. Pan, D. A. Tenne and H. M. Christen, *Adv. Mater.*, 2013, **25**, 5561.
- 23 Y.-J. Wu, X.-K. Chen, J. Zhang and X.-J. Chen, *Physica B*, 2013, **411**, 106.
- 24 Z. Chen, Z. Luo, C. Huang, Y. Qi, P. Yang, L. You, C. Hu, T. Wu, J. Wang, C. Gao, T. Sritharan and L. Chen, *Adv. Funct. Mater.*, 2011, **21**, 133.
- 25 H. Guo, R. Zhao, K. J. Jin, L. Gu, D. Xiao, Z. Yang, X. Li, L. Wang, X. He, J. Gu, Q. Wan, C. Wang, H. Lu, C. Ge, M. He and G. Yang, *ACS Appl. Mater. Interfaces*, 2015, **7**, 2944-2951.
- 26 V. A. Khomchenko, J. A. Paixão, B. F. O. Costa, D. V. Karpinsky, A. L. Kholkin, I. O. Troyanchuk, V. V. Shvartsman, P. Borisov and W. Kleemann, *Cryst. Res. Technol.*, 2011, **46**, 238.
- 27 M. Iliev, M. Abrashev, H.-G. Lee, V. Popov, Y. Sun, C. Thomsen, R. Meng and C. Chu, *Phys. Rev. B*, 1998, **57**, 2872.
- 28 M. V. Abrashev, A. P. Litvinchuk, M. N. Iliev, R. L. Meng, V. N. Popov, V. G. Ivanov, R. A. Chakalov and C. Thomsen, *Phys. Rev. B*, 1999, **59**, 4146.
- 29 S. Jesse, A. P. Baddorf and S. V. Kalinin, *Appl. Phys. Lett.*, 2006, **88**, 062908.
- 30 J. Li, J.-F. Li, Q. Yu, Q. N. Chen and S. Xie, *Journal of Materiomics*, 2015, **1**, 3.
- 31 L.-Q. Cheng, K. Wang, J.-F. Li, Y. Liu and J. Li, *J. Mater. Chem. C*, 2014, **2**, 9091.
- 32 S. Jesse, H. N. Lee and S. V. Kalinin, *Rev. Sci. Instrum.*, 2006, **77**, 073702.
- 33 S. V. Kalinin, A. N. Morozovska, L. Q. Chen and B. J. Rodriguez, *Rep. Prog. Phys.*, 2010, **73**, 056502.
- 34 S. A. Prosandeev, D. D. Khalyavin, I. P. Raevski, A. N. Salak, N. M. Olekhnovich, A. V. Pushkarev and Y. V. Radyush, *Phys. Rev. B*, 2014, **90**, 054110.
- 35 B. Xu, D. Wang, J. Iñiguez and L. Bellaiche, *Adv. Funct. Mater.*, 2015, **25**, 552.

## Journal Name

## ARTICLE

- 36 D. A. Rusakov, A. M. Abakumov, K. Yamaura, A. A. Belik, G. Van Tendeloo and E. Takayama-Muromachi, *Chem. Mater.*, 2011, **23**, 285.
- 37 S. V. Kalinin, B. J. Rodriguez, S. Jesse, P. Maksymovych, K. Seal, M. Nikiforov, A. P. Baddorf, A. L. Kholkin and R. Proksch, *Mater. Today*, 2008, **11**, 16.
- 38 S. E. Reyes-Lillo and K. M. Rabe, *Phys. Rev. B*, 2013, **88**, 180102.
- 39 S. Saxin and C. S. Knee, *Dalton trans.*, 2011, **40**, 3462-3465.
- 40 Y. Y. Liu, L. Yang and J. Y. Li, *J. Appl. Phys.*, 2013, **113**, 183524.
- 41 A. Chaturvedi and V. Sathe, *Thin Solid Films*, 2013, **548**, 75.
- 42 M. N. Iliiev and M. V. Abrashev, *J. Raman Spectrosc.*, 2001, **32**, 805.
- 43 B. C. Jeon, D. Lee, M. H. Lee, S. M. Yang, S. C. Chae, T. K. Song, S. D. Bu, J. S. Chung, J. G. Yoon and T. W. Noh, *Adv. Mater.*, 2013, **25**, 5643.